August 2020

Prepared by Fasmatech & Karolinska Institute

CONTENTS

D2.2 Protocol of in situ testing of the optimized CAD MS/MS

2.2.1 Collisional Activation in the Omnitrap Platform

The Omnitrap platform enables two different types of collisional activation methods. Slow heating collision induced dissociation (CID) is accomplished by applying a resonance excitation signal to the pole-electrodes in segments Q2 and Q5. Beam-type CID can also be performed by accelerating ions axially utilizing the fast switching DC potentials controlling the DC profile across the length of the ion trap. **Figure 1** is concerned with the slow heating CID method and a direct comparison is made between ion traps driven by rectangular and sinusoidal RF waveforms. Simulations results indicate that ion-molecule binary collisions are considerably more energetic in rectangular RF driven systems. The implications of this effect have not been fully explored, however, it is understood that more energetic collisions can impart a greater amounts of energy into the ions in a shorter period of time resulting in faster CID and/or readily dissociating high mass ions with many molecular degrees of freedom. In addition, the relative rates of vibrational excitation and internal energy relaxation, which are the two competing mechanisms in slow heating processes, are altered. Ions experiencing an alternating voltage pulse will accelerate to greater kinetic energies while the transition period through the low velocity regime is minimized. Consequently, a greater number of energetic collisions are established increasing the rate of vibrational excitation whilst the lower number of soft collisions suppresses the rate of internal energy relaxation. **Figure 1** shows phase space diagrams for ubiquitin 8+ ions under resonance excitation conditions. The effective potential wells are calculated for both RF waveforms, while the more energetic conditions are observed in two different pressure regimes.

Overall, slow heating CID in the Omnitrap platform has been performed seamlessly and with high efficiency for many different systems, starting from smaller protein ions like ubiquitin and extending to intact monoclonal antibodies and protein complexes. Here a long list of experiments with ubiquitin is presented together with successful efforts in fragmenting monoclonal antibodies (mAbs). The efficiency of slow heating CID of a mAb is contrasted to HCD fragmentation performed in the Q Exactive platform. In addition, several MS3 CID experiments with radical ions generated either by electron ionization or electron capture have been performed successfully.

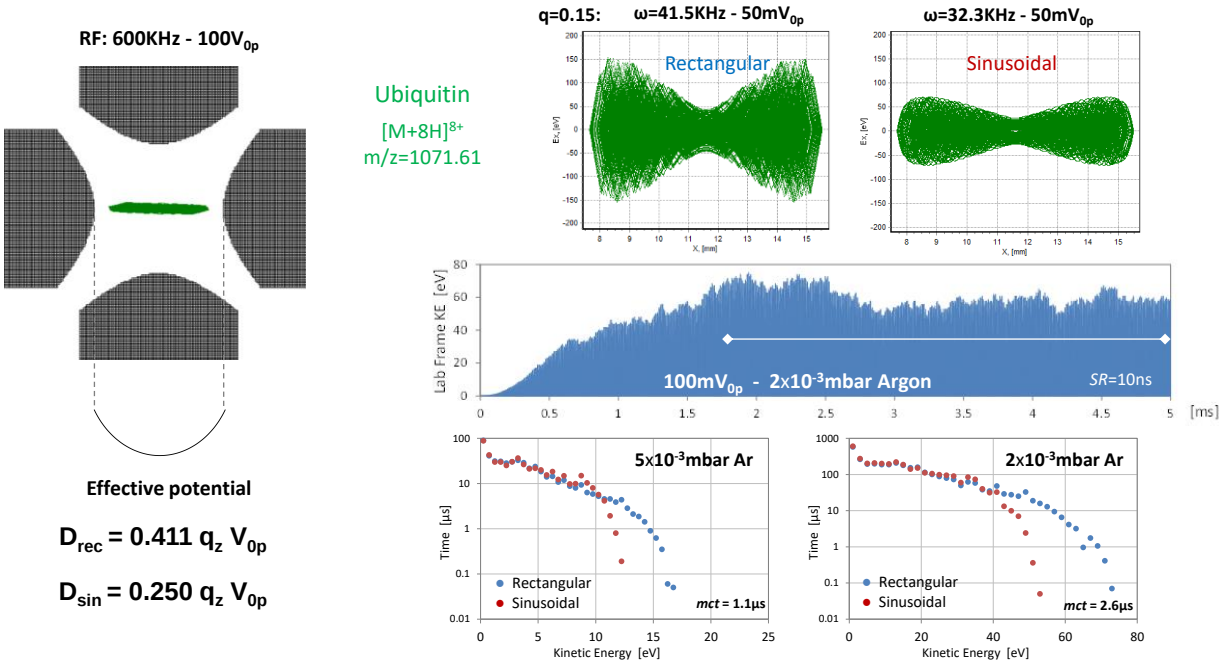

Figure 1. Simulation results of the slow heating CID process performed in rectangular and sinusoidal RF driven ion traps. The more energetic collisions established in the Omnitrap platform are highlighted for the case of ubiquitin 8+ ions.

2.2.2 Slow Heating CID of Ubiquitin

A comprehensive study of slow heating CID using ubiquitin as a test bench system has been performed. Different charge states have been investigated corresponding to the three possible conformational states of ubiquitin. The native 6+ ions are created by preparing ubiquitin in ammonium acetate 100mM. The partially unfolded 8+ ions are created by preparing ubiquitin in water and 1% acetic acid, while the unfolded charge state 12+ is created by using water:methanol:acetic acid in the following ratios 50:49:1. Data processing was performed in Peak Finder, a new software platform developed by Fasmatech and tailored for processing complex top down spectra. Peak Finder utilizes new algorithms for fitting entire isotopic distributions to the experimental data. These calculations are currently performed for known sequences however there is a strong intension to extend the algorithm for de novo sequencing applications. In Peak Finder spectrum deconvolution is eliminated and so is the increasing number of errors associated with such processes for complex and highly congested mass spectra. Experimental results are presented together with MS3 CID of the hydrogen deficient radical ions at the same charge state formed by electron ionization. The following reactions performed in the Omnitrap platform are presented in **Scheme 1**. A list of the compared species and their corresponding charge states are also presented.

Electron Ionization Reactions

$[M+5H]^{5+} + e^- \longrightarrow [M+5H]^{6+\bullet} + 2e^-$

$[M+7H]^{7+} + e^- \longrightarrow [M+7H]^{8+\bullet} + 2e^-$

$[M+11H]^{11+} + e^- \longrightarrow [M+11H]^{12+\bullet} + 2e^-$

CID spectra comparison

$[M+6H]^{6+}$ vs $[M+5H]^{6+\bullet}$

$[M+8H]^{8+}$ vs $[M+7H]^{8+\bullet}$

$[M+12H]^{12+}$ vs $[M+11H]^{12+\bullet}$

Scheme 1. Electron ionization reactions of ubiquitin ions performed to generate the hydrogen deficient species and a list of the different charge states of even and odd electron ubiquitin ions subjected to slow heating CID.

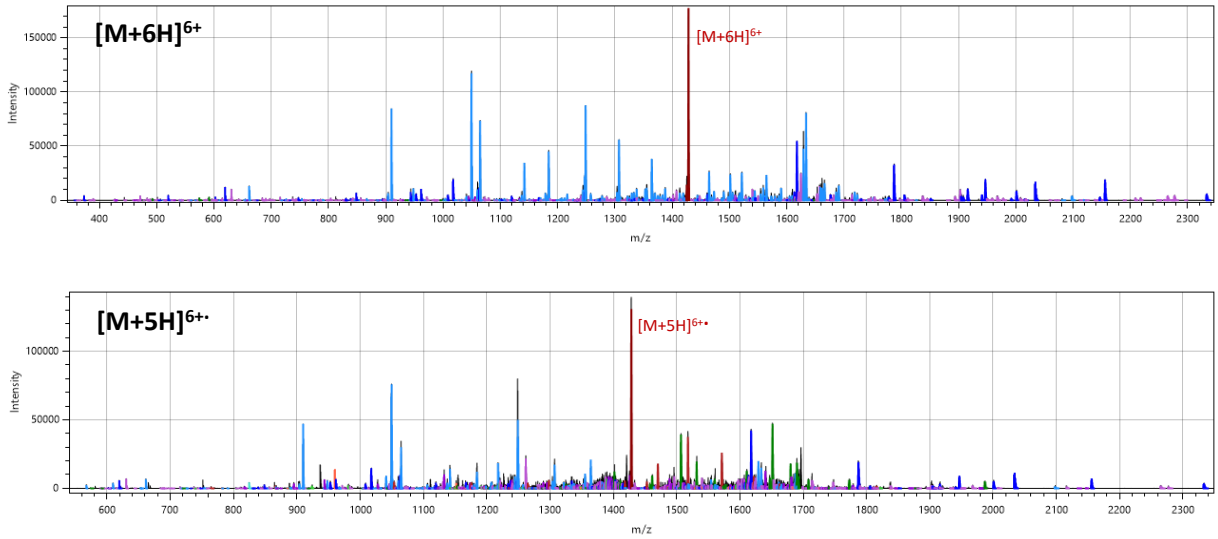

Figure 2. MS2 CID spectra of ubiquitin 6+ and MS3 CID of ubiquitin 6+•. Spectra are processed in Peak Finder. The theoretical isotopic distributions are superimposed on the experimental data.

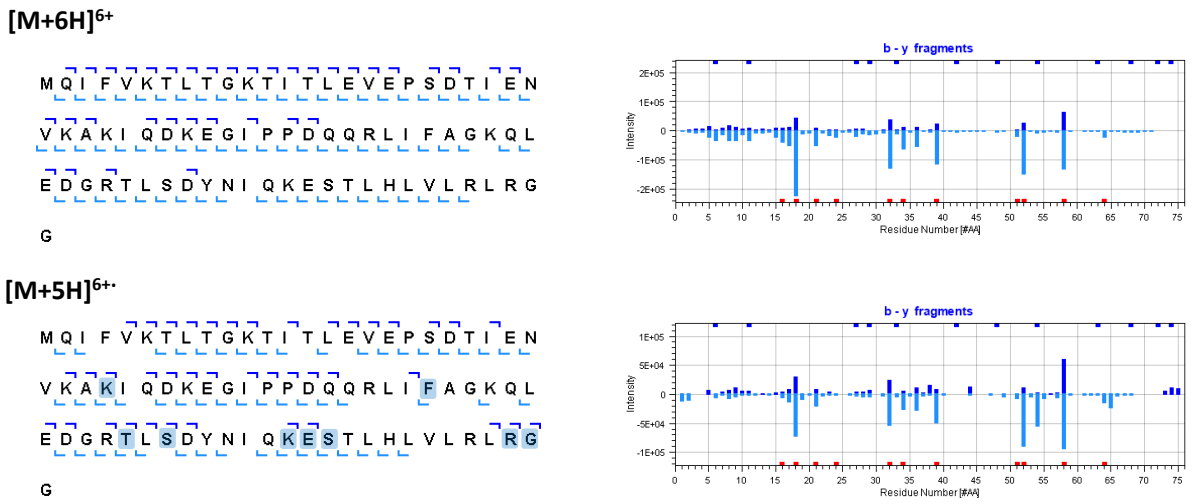

Figure 3. Sequence maps for ubiquitin 6+ and 6+•. Fragment ion intensity graphs indicate regions with preferential cleavages. The additional cleavages observed in MS3 CID of the 6+• species are also highlighted.

Figure 2 and **Figure 3** summarize slow heating CID results for the 6+ and 6+• ions produced in MS2 and MS3 modes respectively. The sequence coverage for the native ubiquitin ion species is very high, however, additional cleavages are observed for the ionized 6+• species. In addition to the c-z and a-x new fragment series observed in the MS3 CID experiments of $[M+5H]^{6+\bullet}$ are presented in **Figure 4** below. Noticeable are differences observed in the b-y fragmentation patterns when comparing $[M+5H]^{6+\bullet}$ and $[M+6H]^{6+}$. For example, new b-type cleavages are observed on the C terminus, and also new b-type cleavages are observed next to residues K29, F45, T55, S57, K63, E63, S65. The y_{22} fragment ion intensity on residue T55 is enhanced. All these new fragments can be associated with residues incorporating the hydroxyl group (–OH) on the side chain, and are therefore capable of donating a H• to the electron hole produced upon electron irradiation. The only new residue appearing in the MS3 CID of $[M+5H]^{6+\bullet}$ and violating this rule is lysine.

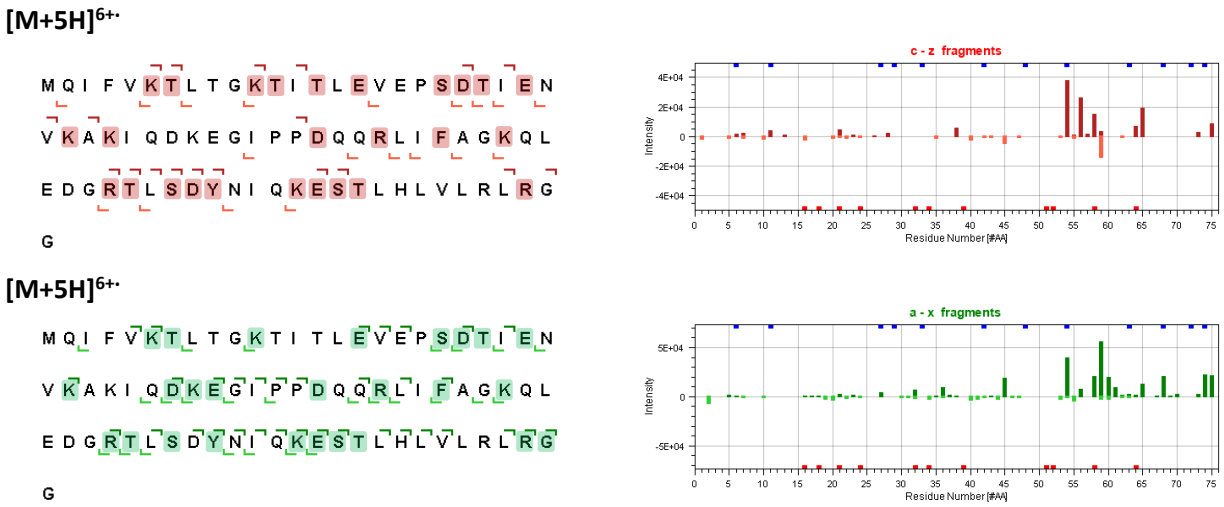

Figure 4. Sequence maps for ubiquitin 6+• highlighting all the new fragments observed for these hydrogen deficient species compared to the 6+ ions. Fragment ion intensity graphs indicate regions with preferential cleavages.

For the $[M+5H]^{6+\bullet}$ a new series of c and z• fragments are observed. These new cleavages appear mostly next to residues, which are likely to be involved in radical chemistry and participate in intramolecular hydrogen atom rearrangement reactions. More specifically, and similarly to the data presented in **Figure 4** for the b and y ions produced from the hydrogen deficient species, the additional c and z• fragments are observed next to aromatic residues F45 and Y59, threonines, T9, T12, T14, T22, T55, T66 (6/7 Thr), serines, S20, S57, S65 (3/3 Ser), at the C-terminus, next to acidic residues, E16, D21, E24, D39, D58, E64 (6/11) and also on basic residues, K6, K11, K27, K29, K48, R54, K63, R74 (8/11 K & R). From all these new fragments listed above, excluding the basic aminoacids (lysine), cleavages are formed next to residues that accommodate a hydroxyl group –OH on ther side chains. Very similar trends are observed for the a and x fragment ions. It is understood that the hydroxyl groups can donate a hydrogen atom H• to the electron hole. The initiation of the intramolecular transfer process following the generation of an electron hole is considered responsible for the rich fragmentation pattern observed for these residues. Beyond the extremely interesting fundament aspect underlying these processes, the sequence information for the

radical ubiquitin ions is greatly enhanced compared to even electron species. Despite the reduction, the signal-to-noise ratio is at least by one order of magnitude, which is attributed to operating the Omnitrap platform in MS3 mode. **Figure 5** summarizes results from six separate CID experiments performed in the Omnitrap platform

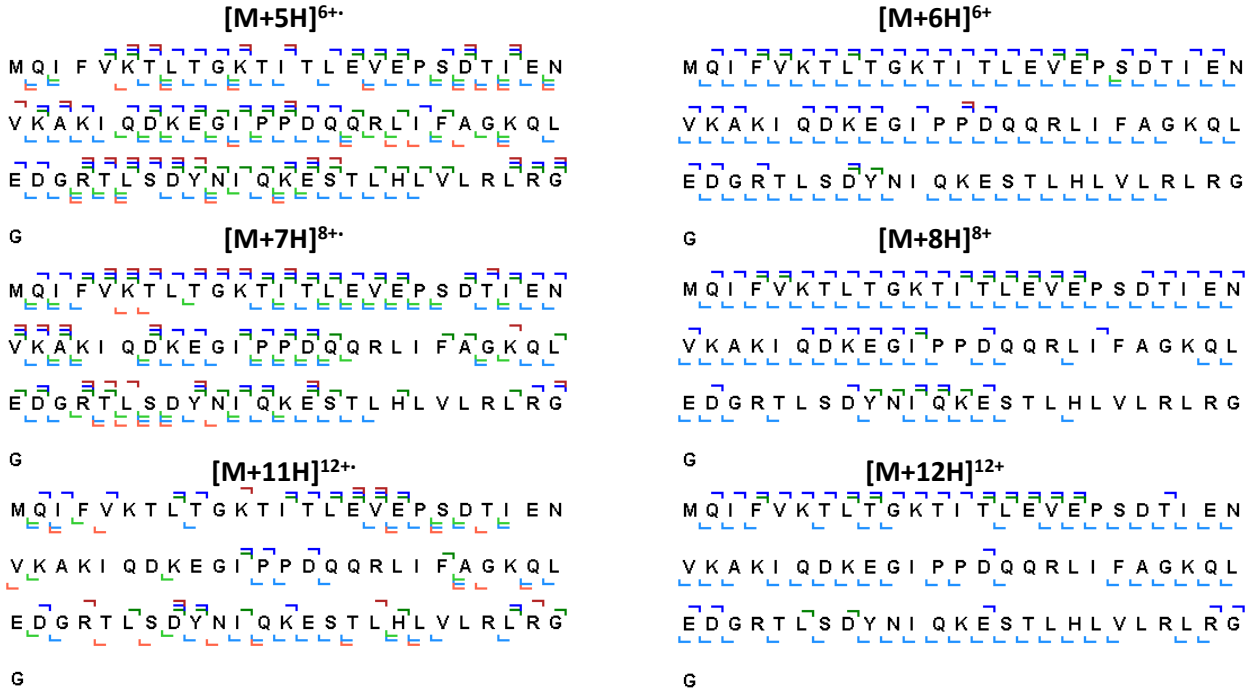

Figure 5. Sequence maps for ubiquitin comparing MS2 CID of the even electron species and MS3 CID of the odd electron species. Results demonstrate the formation of entirely new sets of fragments observed for the hydrogen deficient ions and further highlight the rich chemistry exhibited by these radical species, which can also lead to enhanced sequence information.

2.2.3 Slow Heating CID of denatured Herceptin

Two different types of CID experiments have been performed in the Omnitrap platform for the analysis of denatured and native Herceptin (trastuzumab) samples. **Figure 6** shows the part of the ion activation network employed so far in these analyses. The fragmentation pattern observed for the intact mAb is also presented. Results on ECD will be omitted in this report, however highly efficient collisional activation of ECD charge reduced ions has been performed.

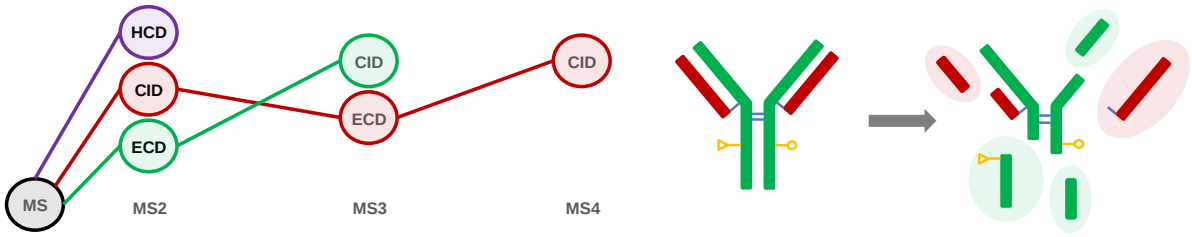

Figure 6. Ion activation network employed and observed fragmentation pattern of the intact mAb.

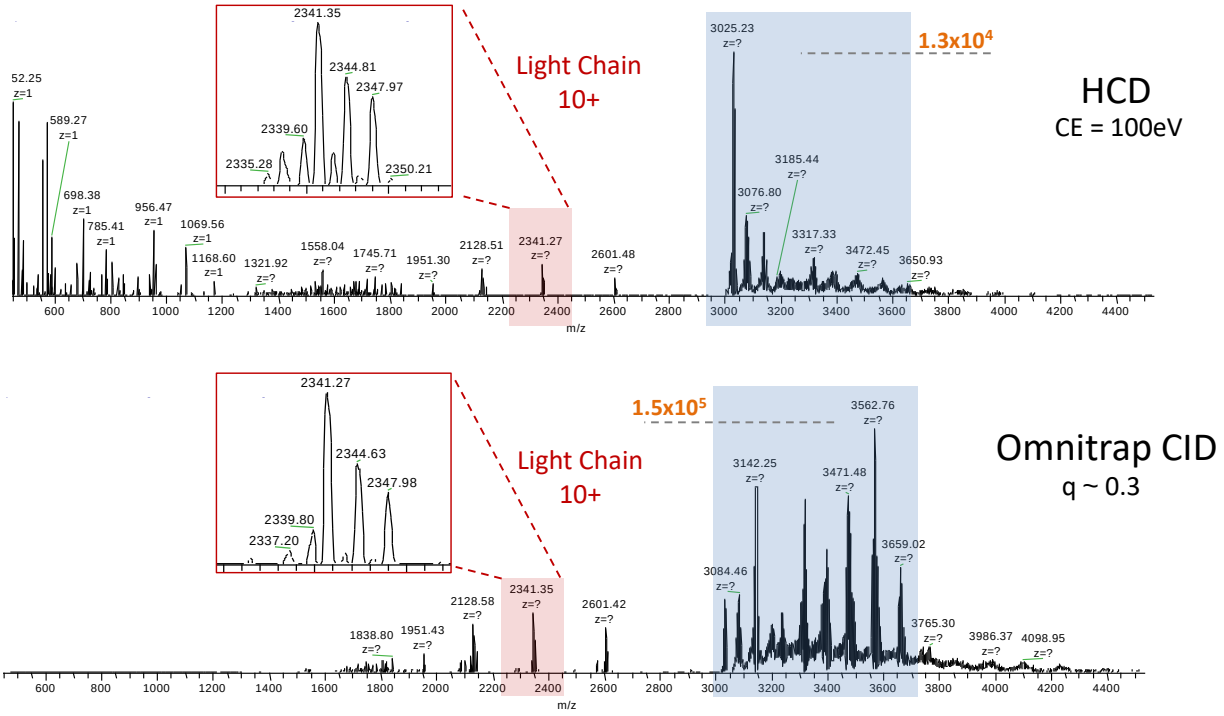

Figure 7. HCD and slow heating CID in the Q Exactive Plus (Biopharma) and in segment Q2 of the Omnitrap platform of intact Herceptin 49+ produced under denatured conditions. The Orbitrap analyzer is operated in low resolution mode. The light chain subunit fragment is observed and highlighted in both spectra.

Figure 7 compare HCD and CID spectra produced at optimized conditions in the Q-Exactive Plus and in the Omnitrap platform, respectively. The intensity of the HCD spectrum is one order of magnitude lower compared to the intensity of the spectrum produced in segment Q2 of the Omnitrap platform. This difference is partly attributed to ion losses induced by the fringe-fields at the exit lens of the HCD cell, which can have a sever effect on low q_z ions. Another important parameter is the significant difference in

the pressure regime where collisional activation is exercised. Pulsing gas in the Omnitrap provides access to elevated pressure exceeding $5x10^{-2}$ mbar. Fragments formed upon resonance excitation will fall off resonance and will experience thermalizing collisions relaxing to the central axis of the ion trap. In contrast, the HCD cell produces a far richer spectrum on the low mass side partly due to secondary ion fragmentation processes, which are absent under resonance excitation conditions, and also partly due to the higher low-mass cut-off settings applied to the Omnitrap for this particular experiment.

Figure 8 shows the HCD spectrum of the 49+ Herceptin ions plotted in Peak Finder together with the theoretical isotopic distributions of the assigned fragments. The sequence map is also presented with 7.5% sequence coverage obtained for the light chain and 6.5% sequence coverage obtained for the heavy chain. 62% of the total ion intensity is assigned to primary fragment ions. A significant number of internal fragment ions have been identified raising the total signal assigned to 79%. In the mass spectrum internal fragments are highlighted in purple while the charge states of the light chain in red.

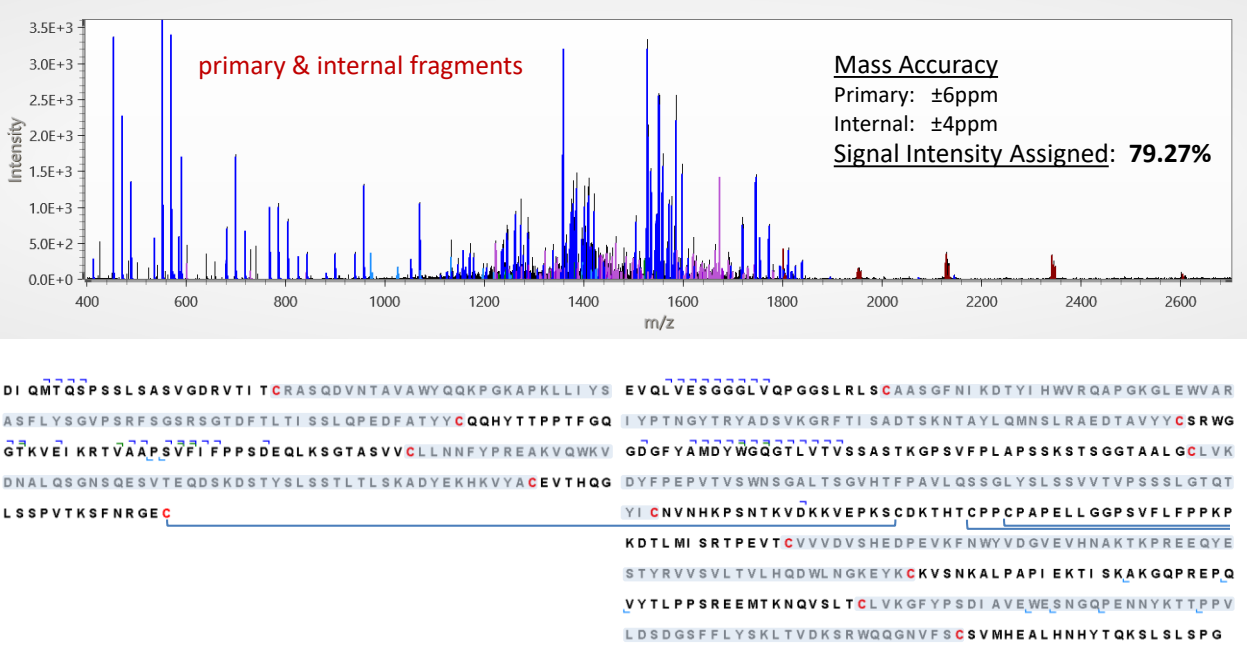

Figure 8. HCD spectrum of denatured Herceptin analyzed under non-reducing conditions and sequence map.

Figure 9 highlights the multiple cleavages observed across the disulfide bridge connecting the two mAb chains. The exact same fragmentation pattern is observed in HCD fragmentation performed in the Q-Exactive Plus. Here there is no evidence of asymmetric charge partitioning since the charge state of the light chain is rather low compared to the charge state of the precursor. This can be attributed to the stable S-S bonds present in the light chain maintaining the structure of the protein subunit during fragmentation.

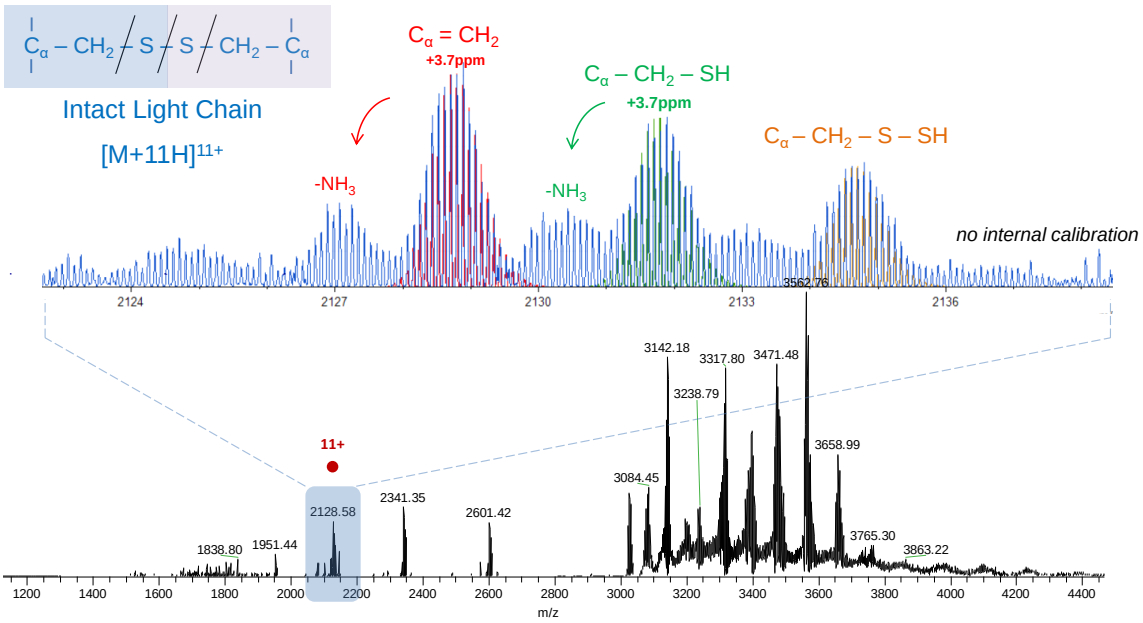

Figure 9. Slow heating CID spectrum of Herceptin highlighting the multiple cleavages observed across the S-S bridge connecting the two mAb chains.

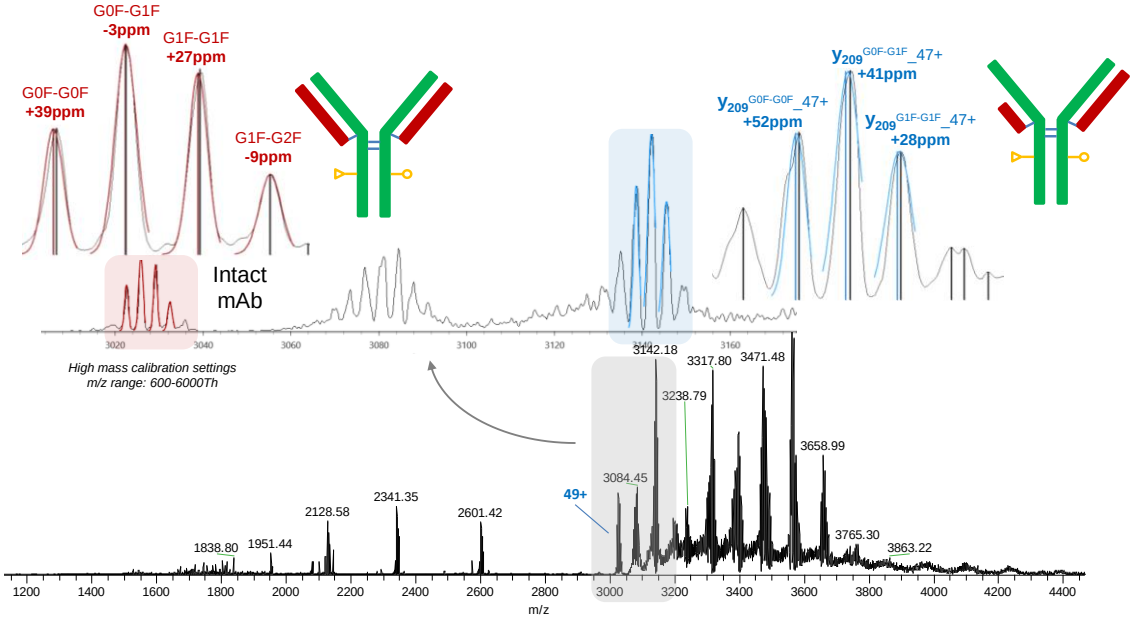

Figure 10. Slow heating CID spectrum of Herceptin highlighting the multiple cleavages observed across the S-S linkage.

Figure 10 demonstrates yet another interesting feature of the slow heating CID spectrum of the 49+ Herceptin ions. Despite the low mass accuracy at the higher m/z values, several assignments where made with high confidence, mainly due to the identification of the lower m/z complementary ions. In this example, the glycosylated profile of a high mass fragment is highlighted and identified as the truncated mAb fragment containing the two heavy chains, one light chain and the truncated light chain in the form of a y-type fragment connected to one of the heavy chains through an S-S bond. Identification of the high mass fragments is a tedious task and cannot be performed efficiently due to the unresolved isotopic patterns and due to the lower mass accuracy in this m/z range.

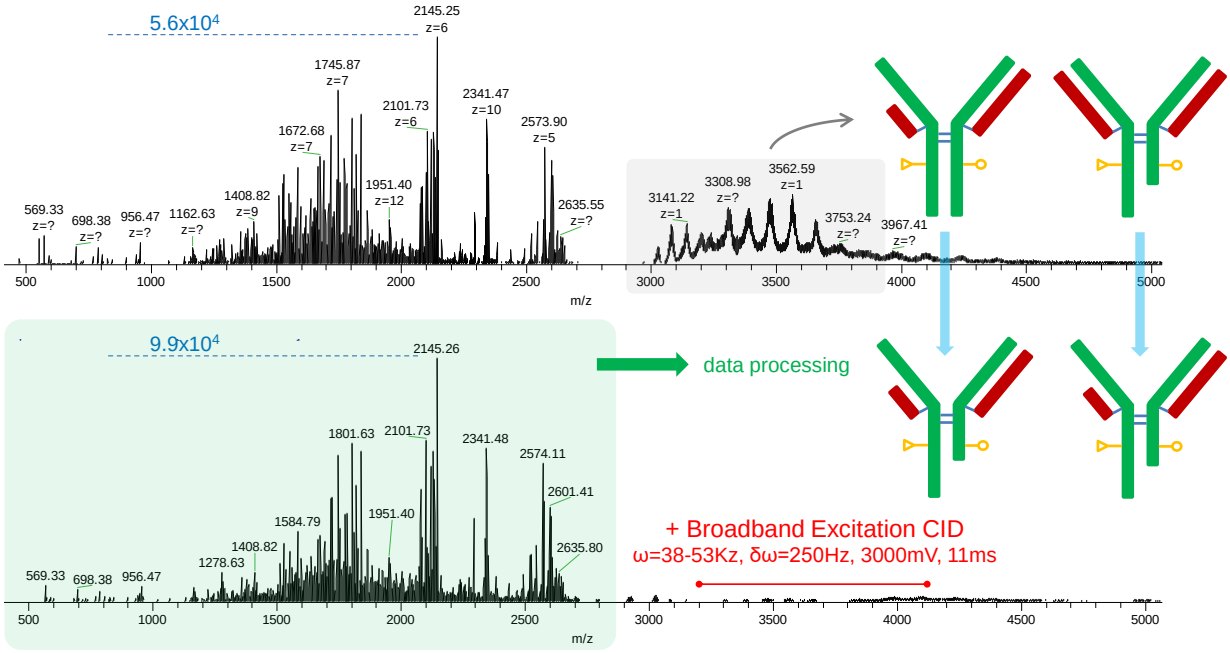

Figure 11. Slow heating CID spectrum of Herceptin followed by broadband excitation of the high mass fragments (truncated antibodies), which enhances the signal-to-noise ratio of the CID fragments by a factor of 2x.

Operating the Orbitrap mass analyzer in high resolution mode (240,000) produces spectra with isotopically resolved fragments up to m/z ~3000. **Figure 11** shows the high resolution slow heating CID spectrum of Herceptin charge state 49+. Also shown is the spectrum produced following the application of a broadband excitation signal with excitation frequencies corresponding to the truncated mAbs observed at m/z>3000Th. Careful analysis of the results has shown that this additional step of collisional activation in the presence of a consecutive gas pulse does not produce additional fragments. Surprisingly, broadband excitation CID of the truncated mAbs will only increase the signal of the exact same fragment

ions produced during the first step of slow heating CID. An attempt to explain this effect is made in **Figure 11** showing the dissociation pathways of the truncated mAb units. During the first CID step, an intact mAb will lose an N-terminal fragment from the light chain or a C-terminal fragment from the heavy chain. Subjecting these truncated mAB units to a consecutive step of collisional activation will result in the formation of additional fragments which will follow the same dissociation pathways with those exhibited by the intact mAb. Consequently, a truncated mAb unit losing an N-terminal fragment from the light chain in the first step of slow heating CID will lose a C-terminal fragment in the second consecutive step of collisional activation and vice versa. It is not clear yet whether the doubly truncated mAb units produced following the application of the broadband excitation signal will produce additional fragments outside the m/z range examined in these experiments (m/z>5000Th).

Before post processing the CID+Broadband excitation spectrum of the 49+ Herceptin ions in Peak Finder, internal calibration was performed in mMass. **Figure 12** shows the ppm error before and after calibrating the mass spectrum using a short list of fragments identified manually. The mass accuracy error after the internal calibration is ±3ppm, while all fragments after the assignment is completed are confined within ±6ppm.

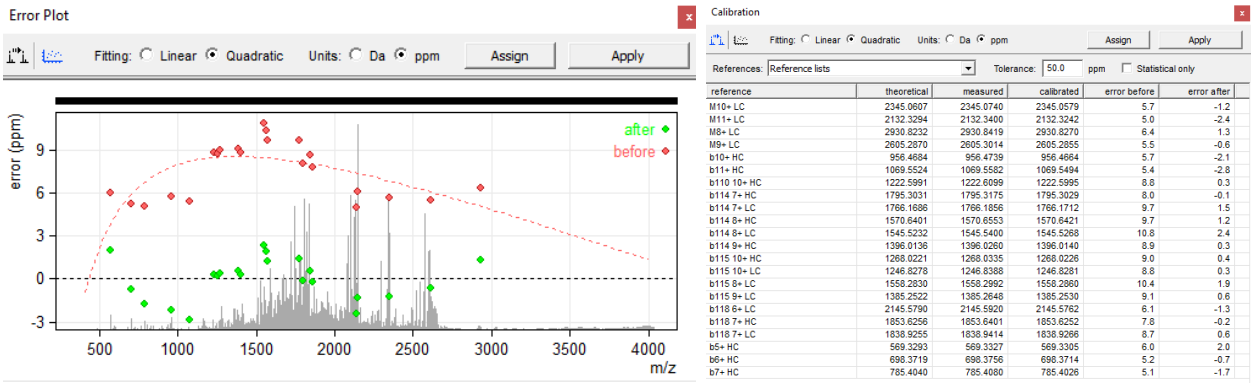

reference	theoretical	measured	calibrated	error before	error after
M10+ LC	2345.0607	2345.0740	2345.0579	5.7	-1.2
M11+ LC	2132.3294	2132.3400	2132.3242	5.0	-2.4
M8+ LC	2930.8232	2930.8419	2930.8270	6.4	1.3
M9+ LC	2605.2870	2605.3014	2605.2855	5.5	-0.6
b10+ HC	956.4684	956.4739	956.4664	5.7	-2.1
b11+ HC	1069.5524	1069.5582	1069.5494	5.4	-2.8
b110 10+ HC	1222.5991	1222.6099	1222.5995	8.8	0.3
b114 7+ HC	1795.3031	1795.3175	1795.3029	8.0	-0.1
b114 7+ LC	1766.1686	1766.1856	1766.1712	9.7	1.5
b114 8+ HC	1570.6401	1570.6553	1570.6421	9.7	1.2
b114 8+ LC	1545.5232	1545.5400	1545.5268	10.8	2.4
b114 9+ HC	1396.0136	1396.0260	1396.0140	8.9	0.3
b115 10+ HC	1268.0221	1268.0335	1268.0226	9.0	0.4
b115 10+ LC	1246.8278	1246.8388	1246.8281	8.8	0.3
b115 8+ LC	1558.2830	1558.2992	1558.2860	10.4	1.9
b115 9+ LC	1385.2522	1385.2648	1385.2530	9.1	0.6
b118 6+ LC	2145.5790	2145.5920	2145.5762	6.1	-1.3
b118 7+ HC	1853.6256	1853.6401	1853.6252	7.8	-0.2
b118 7+ LC	1838.9255	1838.9414	1838.9266	8.7	0.6
b5+ HC	569.3293	569.3327	569.3305	6.0	2.0
b6+ HC	698.3719	698.3756	698.3714	5.2	-0.7
b7+ HC	785.4040	785.4080	785.4026	5.1	-1.7

Figure 12. Internal calibration is performed in mMass using a short list of fragments identified manually and spanning across the m/z range of interest.

Figure 13 shows the mass spectrum with all the assignments including primary and internal fragments which is raising the signal intensity assigned to theoretically calculated isotopic distributions to ~73%. The ppm error for all the identified fragments is also shown. It is emphasized that these data sets are cured manually, that is, after automated processing is completed, careful analysis is performed removing false positives and also adding new information in regions where automated processing was not successful. **Figure 14** shows the sequence map where 24.3% sequence coverage for the light chain and 16.7% sequence coverage for the heavy chain are accomplished. Two S-S bond cleavages are observed, the first connecting light and heavy chains, and the last S-S bond in the Fc part of the antibody. Fragment ion intensities and charge state distribution plots as function of residue number are presented in **Figure 15** for both the light and heavy chains of intact Herceptin.

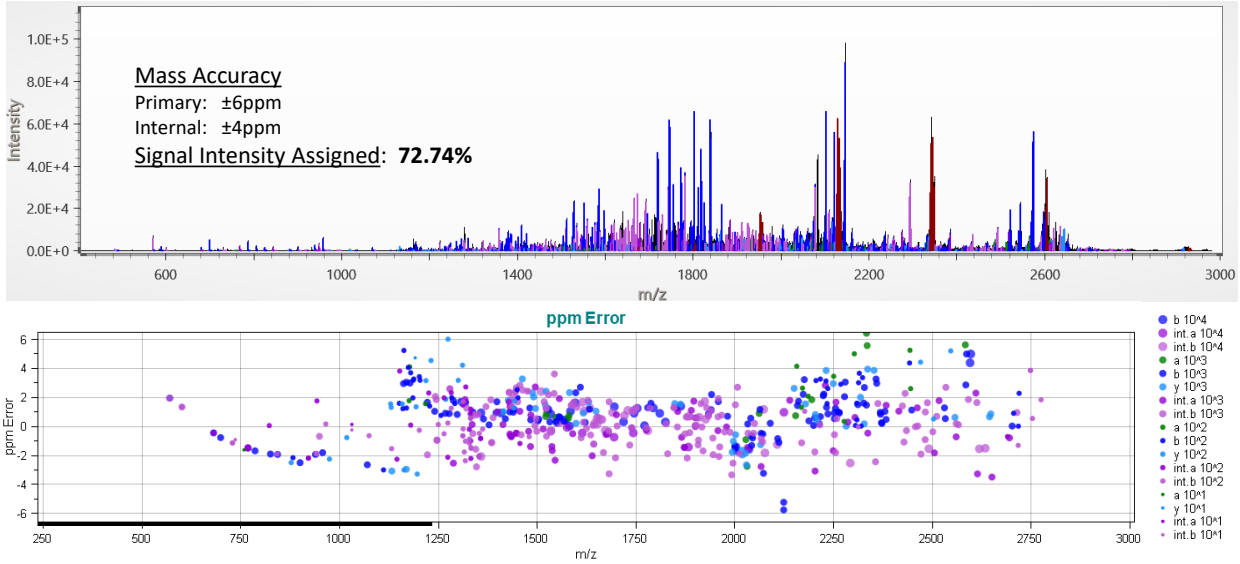

Figure 13. CID+Broadband excitation mass spectrum of Herceptin charge state 49+ with superimposed theoretical isotopic distributions of all primary and internal fragments identified in Peak Finder. The mass accuracy error is confined within ±6ppm.

Figure 14. Sequence map of Herceptin charge state 49+ corresponding to the CID+Broadband excitation mass spectrum of Figure 13. The sequence coverage is 24.3% for the light chain and 16.7% for the heavy chain.

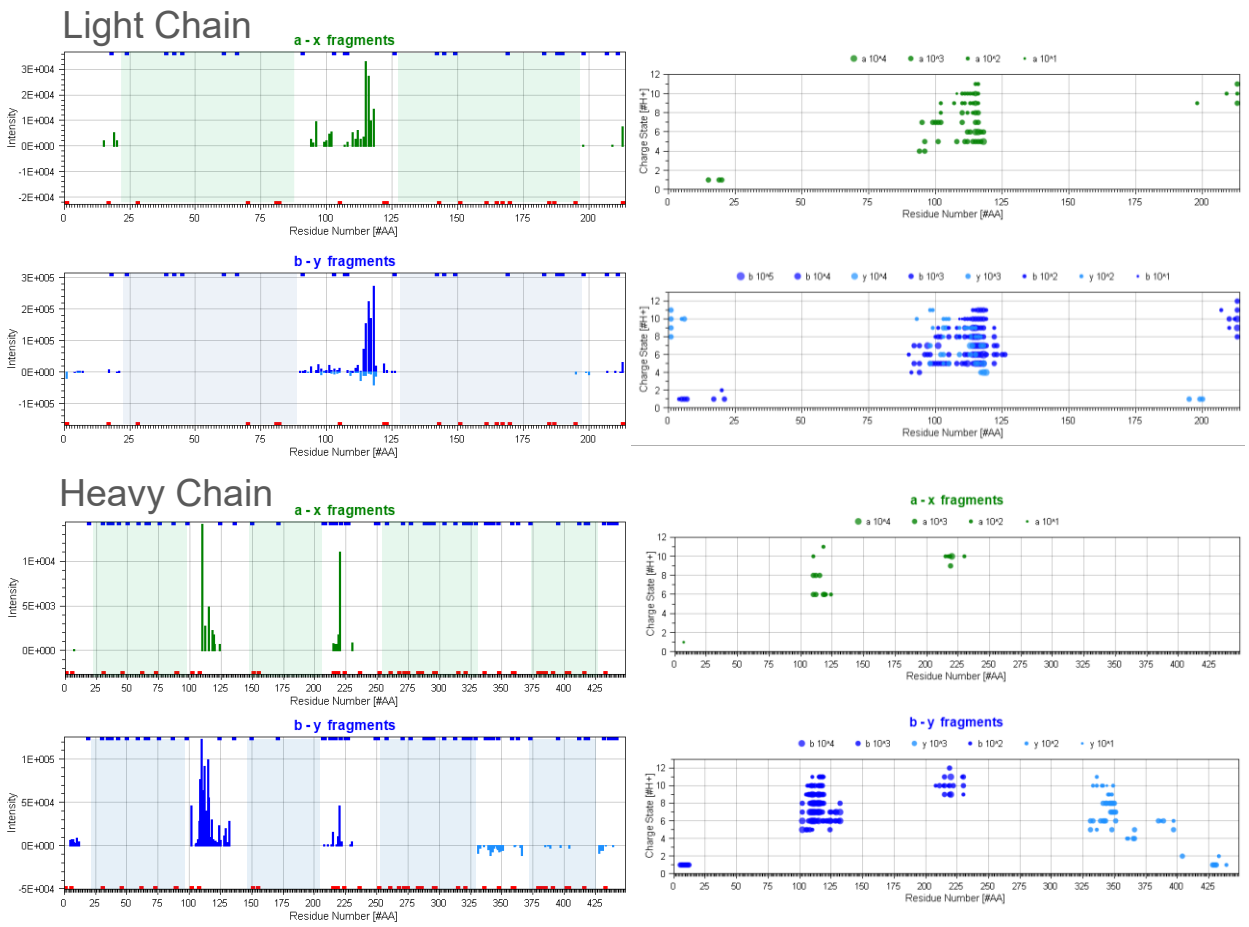

Figure 15. Fragment ion intensities and charge state distribution plots as function of residue number for the light and heavy chains of Herceptin.

The charge state distribution plots provide information as to the number of the different charge states a fragment ions is formed. Fragment ions in the variable region of the heavy chain are observed with as many as seven different charge states.

The detailed analysis of the CID+Broadband excitation spectrum was extended to internal fragments. Calculations have shown that the number of possible internal fragments of an intact mAb can be at least two orders of magnitude greater than the number of primary fragments, without considering side chain losses. A comprehensive data analysis must therefore consider internal fragment formation carefully. Exclusion lists are applied to filter out internal fragments across a disulfide bridge, e.g. fragment with N-terminus side within a disulfide bridge and C-terminus side external to a disulfide bridge. Internal fragments extending from within a first disulfide bridge to within a second disulfide are also filtered out. **Figure 16** shows the internal fragments identified with a mass accuracy of ±4ppm. A significant number of internal fragments have also been matched to isotopic distributions assigned to primary ions. The primary fragments were chosen over internal fragments as the correct assignment in all these cases.

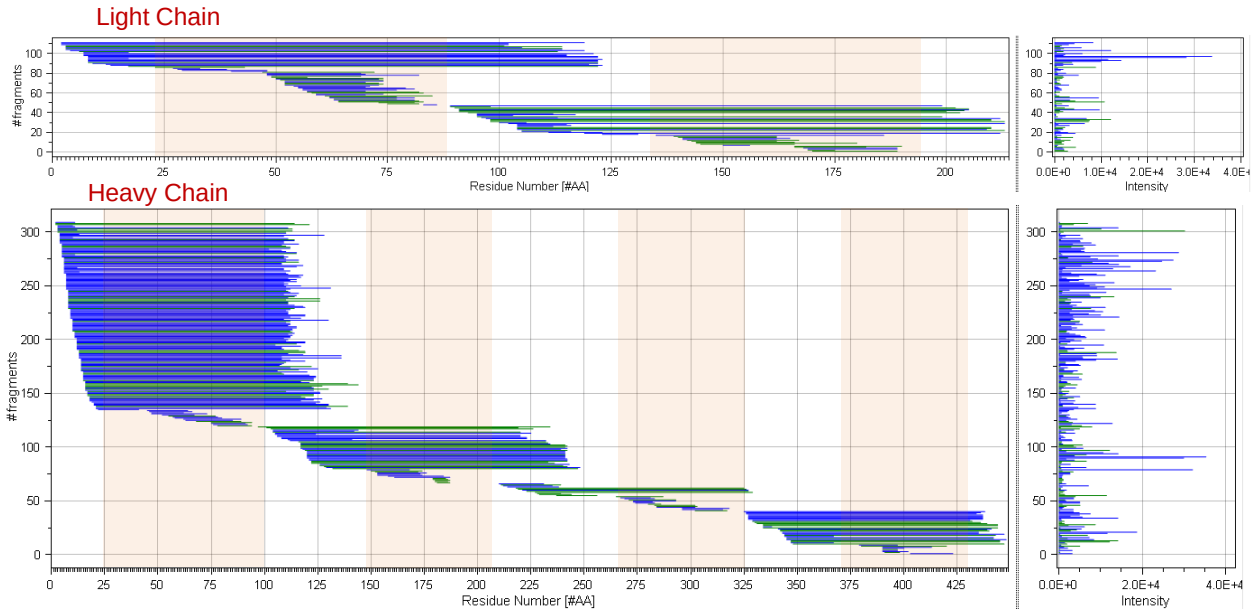

Figure 16. Internal fragments identified in the CID+Broadband excitation spectrum of the denatured non-reduced Herceptin 49+ charge state.

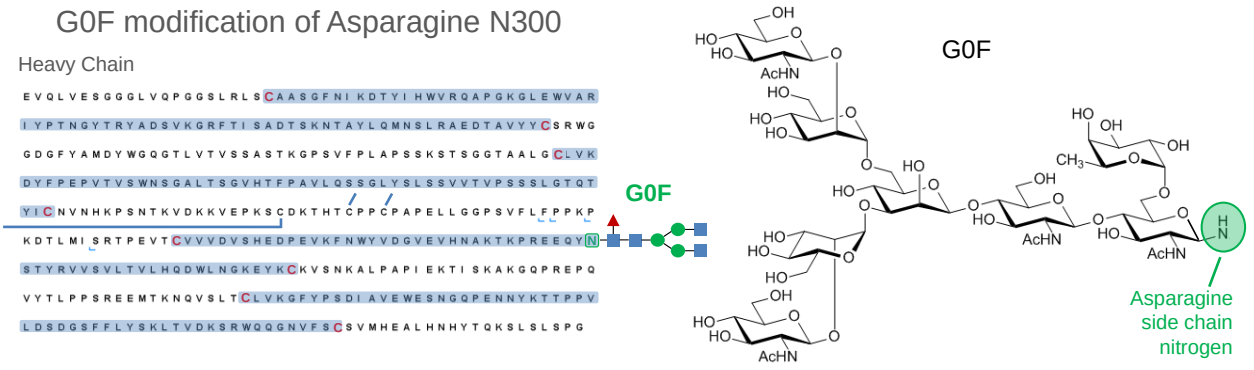

Figure 17. y-type cleavages in the region between the second and the third disulfide bridges containing the G0F glycan modification are identified. These cleavages are formed after the SS bond linking light and heavy chains together and also after the SS bond pair connecting the two heavy chains together.

C-terminus fragments incorporating the glycan modifications are also searched using Peak Finder. A series of y ions before position N-terminus Asp-300 (and Cys-314) are identified near proline residues. No b ions carrying the glycan modification are observed, presumably due to the hinge connection to the second heavy chain. The heavy chain sequence highlighting the few y fragments identified with the G0F modification are presented in **Figure 17**. A few fragments containing the G1F modification are also identified. **Figure 18** shows theoretical isotopic distributions containing the G0F modification superimposed on the experimental data. All isotopic distributions identified with the glycan modification are low intensity and the assignments where made manually. Automated identification of these ions

without introducing false positive matches is a challenging task. Efforts to identify singly charged glycan ions or any of the fragments where unsuccessful.

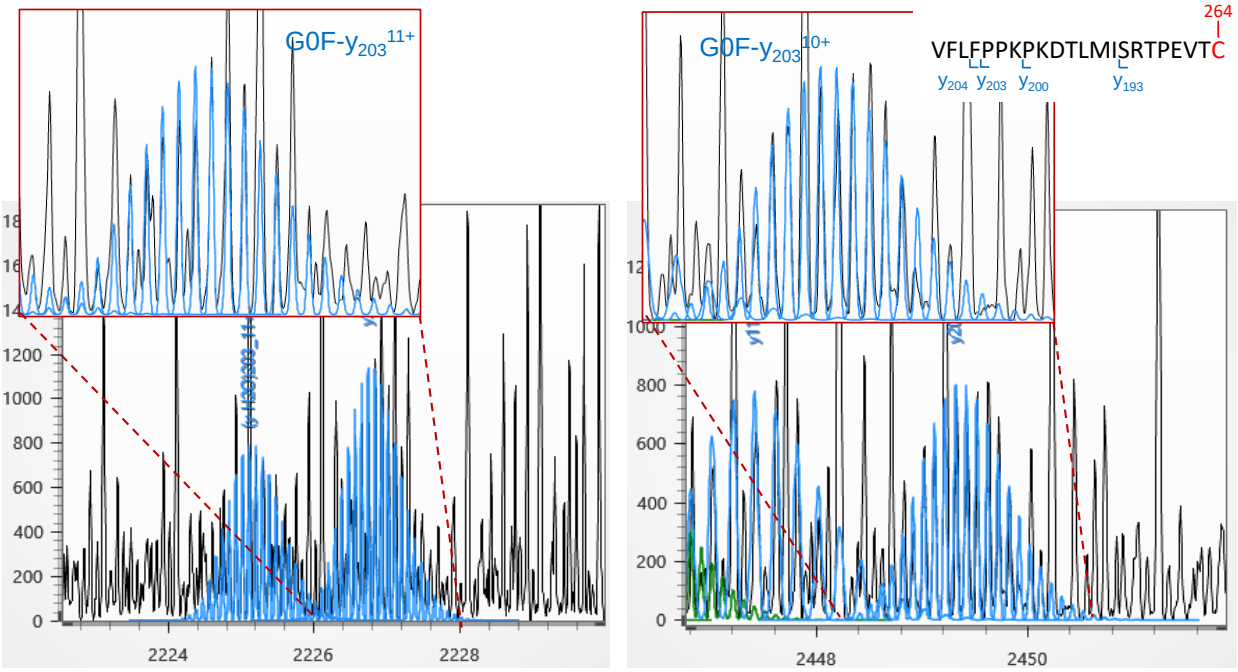

Figure 18. Theoretical isotopic distributions containing the G0F modification superimposed on the CID+Broadband excitation spectrum of Herceptin 49+ charge state.

2.2.4 Slow Heating CID of native Herceptin

CID experiments with native Herceptin charge state 25+ is also performed. Isolation of higher m/z charge state in segment Q2 of the Omnitrap platform are presented in **Figure 19**. Similarly, in the following experiment a resolving DC signal was applied to isolate the 25+ precursor ions. **Figure 20** shows the CID spectra of intact Herceptin sprayed under native conditions. The first spectrum is produced by applying a dipolar excitation waveform during a gas pulse producing fragment ions on either side of the spectrum. Since the higher m/z ions cannot be isotopically resolved and peak assignments are rather difficult to make, an additional broadband excitation signal was applied to dissociate these ions further. Here again application of the broadband excitation waveform enhances the signal-to-noise of all the fragments generated during the first CID step but does not produce new information.

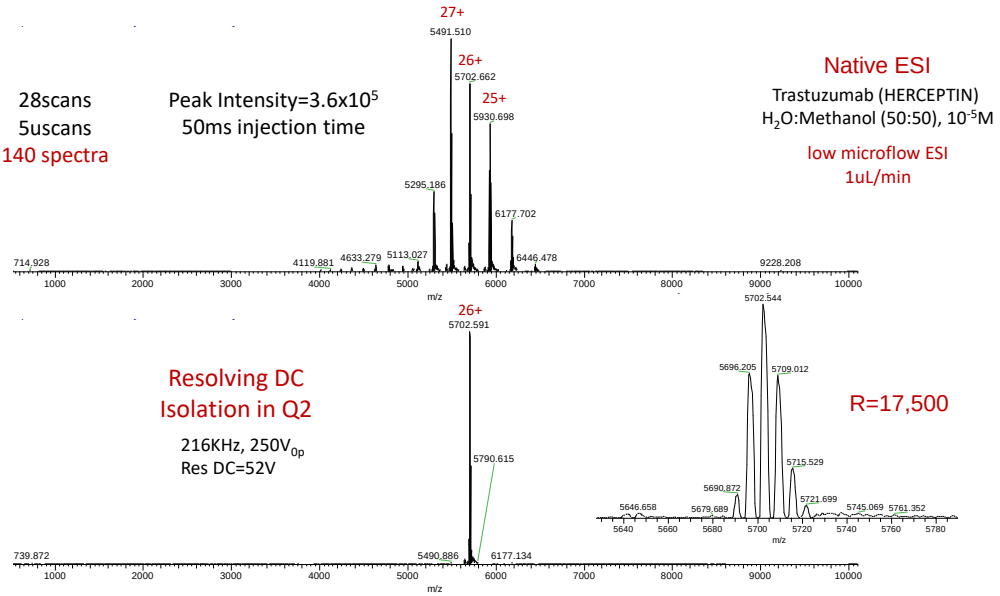

Figure 19. Mass spectrum of Herceptin sprayed under native conditions and resolving DC isolation of charge state 26+. The glycosylation profile is also highlighted.

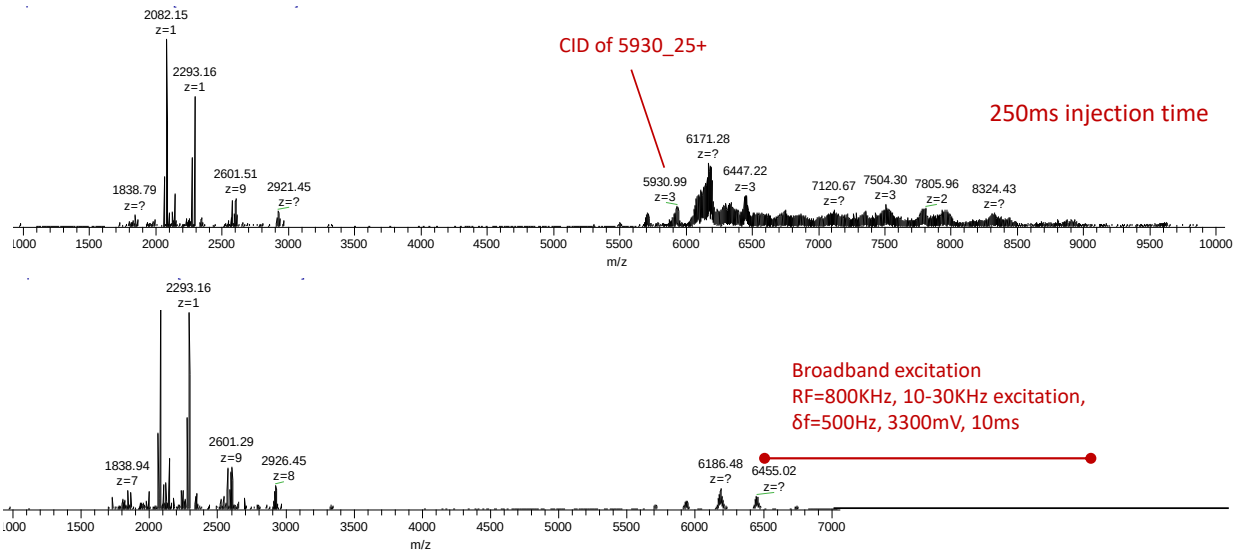

Figure 20. CID spectrum of native Herceptin charge state 25+ followed by a broadband excitation spectrum applied across the higher m/z fragments to enhance signal-to-noise ratio of the first generation CID fragments.

Figure 21 shows the CID+Broadband excitation spectrum of Herceptin charge state 25+ including the theoretical isotopic distributions assigned with a ±6ppm mass accuracy. Interestingly, the light chain subunit is one of the major dissociation pathways observed with charge states similar to those observed

under denaturing conditions. This effect resembles the asymmetric charge partitioning process observed in the dissociation of protein complexes where a monomer subunit is ejected with a disproportional higher number of charge states compared to the remaining complex. This effect can be particularly useful in MS3 mode where the light chain can be further isolated and fragmented by ECD or any of the other methods available in the Omnitrap platform since the number of dissociation pathways under native conditions are significantly less and the intensity of individual fragment ions is greater.

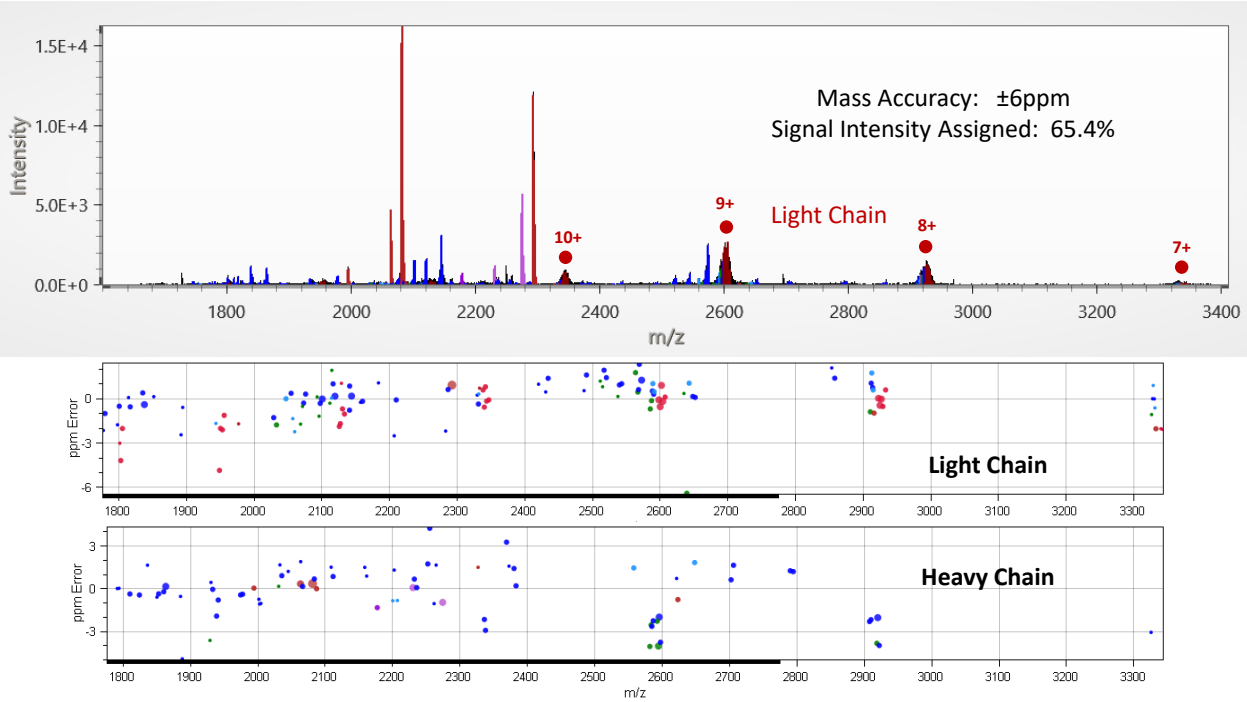

Figure 21. CID spectrum of native Herceptin charge state 25+ including theoretical isotopic distributions of identified fragments with a ±6ppm mass accuracy. The light chain fragments are highlighted.

The sequence coverage obtained under native conditions is presented in **Figure 22**, while charge state distribution plots and ion intensities as a function of residue number are shown in **Figure 23** for b fragments.

Light Chain Sequence Coverage

a : 3.3% x : 0%
b : 5.1% y : 1.9%
c : 1.4% z : 0%
Total: **8.4%**

Heavy Chain Sequence Coverage

a : 0.9% x : 0%
b : 4.2% y : 0.9%
c : 1.1% z : 0.9%
Total: **5.8%**

Figure 22. Sequence map and sequence coverage statistics of Herceptin charge state 25+ sprayed under native conditions. Fragmentation involves a first CID step followed by a broadband excitation signal to fragment the higher m/z first generation product ions further.

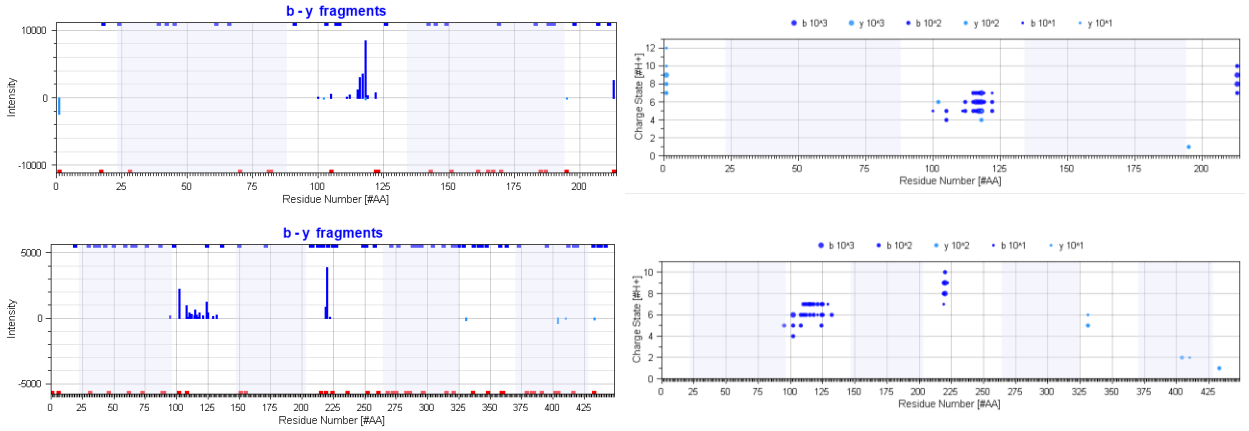

Figure 23. b fragment ion intensities and charge state distribution plots for the CID+broadband excitation spectrum of Herceptin charge state 25+ produced under native ESI conditions.

Another interesting observation made with respect to this CID experiment with an intact mAb sprayed under native conditions is the high ion intensity of c-type fragments forming on the N-terminus side of the first cysteine participating in the SS-bond in both the heavy and light chains. It is emphasized that these high intensity ions are ideal candidates for high quality MS3 experiments that can greatly enhance sequence coverage in regions of interest.

2.2.5 Summary and Outlook

CID experiments of an intact non-reduced mAb sprayed under native and denatured conditions have been performed successfully. In both cases, an additional broadband excitation signal is applied to further fragment the isotopically non-resolved higher m/z species and shown to enhance the signal-to-noise ratio of the first generation fragments. New fragmentation channels are reported with the release of the light chain following the dissociation of the SS bond connecting the two chains being particularly useful for setting up MS3 experiments of selected fragments. In the following example discussed with reference to **Figure 24**, charge state 10+ of the light chain produced by CID is isolated and subjected to ECnoD. Charge reduced ions are subsequently subjected to a collisional activation step by applying excitation frequencies tailored to their respective m/z values. Unfortunately, the resulting MS3 collisionally-activated electron capture dissociation (CA-ECD) spectrum can only be partially processed due to the presence of a residual set of ions leaking from the upstream optics of the Q-Exactive instrument. Nevertheless, processing of this MS3 CA-ECD spectrum shows that both SS bonds of the light chain have been reduced and sequence information from within the disulfide bridges becomes accessible, as shown in **Figure 25**.

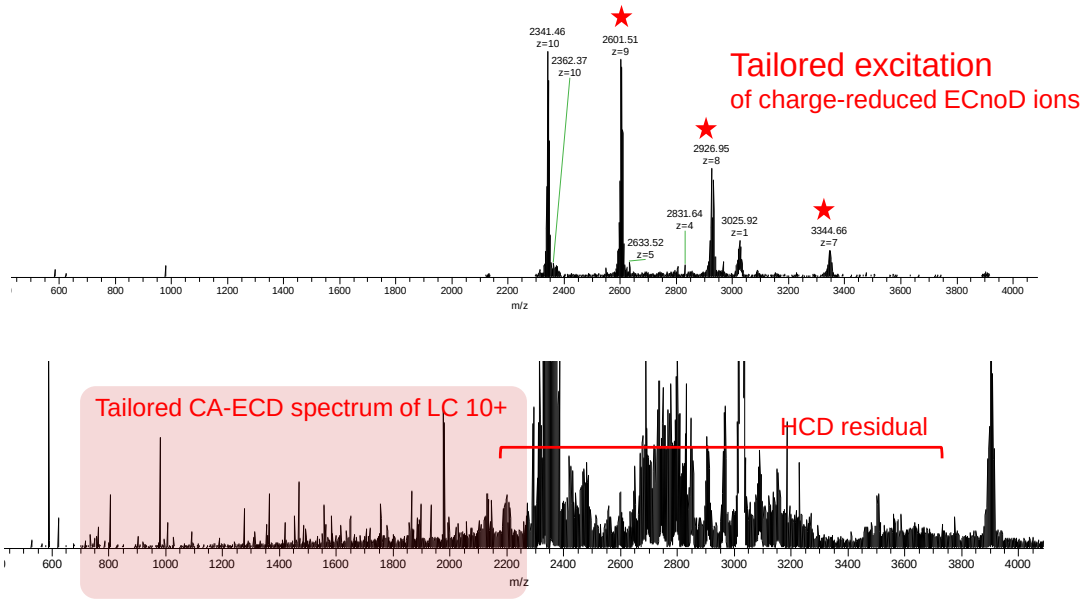

Figure 24. MS3 CA-ECD spectrum of the light chain partially buried under and a set of residual ions leaking from upstream optics of the Q-Exactive instrument.

Figure 25. Sequence map of the light chain produced in an MS3 CA-ECD experiment.

The MS3 mode described above is a highly promising method for obtaining complete sequence coverage of intact mAbs in top down mass spectrometry. In this example three collisional activation steps have been employed successfully, namely, a first CID step using a single excitation frequency followed by the application of a second broadband excitation waveform and, finally, a collisional activation step applied to the charge reduced ions of the light chain following electron capture.

For this mode of operation to become truly useful, an accumulation step is required to enhance the signal-to-noise of product ions. It was found experimentally that the most efficient way of producing high quality MS3 spectra is by enriching the population of the light chain prior to the electron capture event. **Figure 26** shows how the signal of the ions is reduced in each processing step performed in the Omnitrap platform. A signal reduction of nearly two orders of magnitude is observed in the first CID step due to the very high number of dissociation pathways. The signal is partially recovered at the MS3 level by accumulating ions in segment Q8. This is obviously performed at the expense of duty cycle since multiple cycles of fragmentation are required to enrich the ion population prior to mass analysis.

These experiments show that realization of the TopSpec goal to provide an analytical platform for complete sequencing of intact mAbs in top down mode is within reach. Instrumentation problems are currently limiting the very high sequencing coverage of the Herceptin light chain, however, the method described with reference to **Figure 26** shows a possible route to success. This type of experiment can be extended to first generation high-intensity CID fragments of the heavy chain containing the variable region. Resolving the instrumentation problem with the residual ions currently prohibiting the demonstration of enhanced sequence coverage is a priority. Expanding the MS3 accumulation mode to the other ion activation available in the Omnitrap platform holds great promise for the comprehensive analysis of intact antibodies.

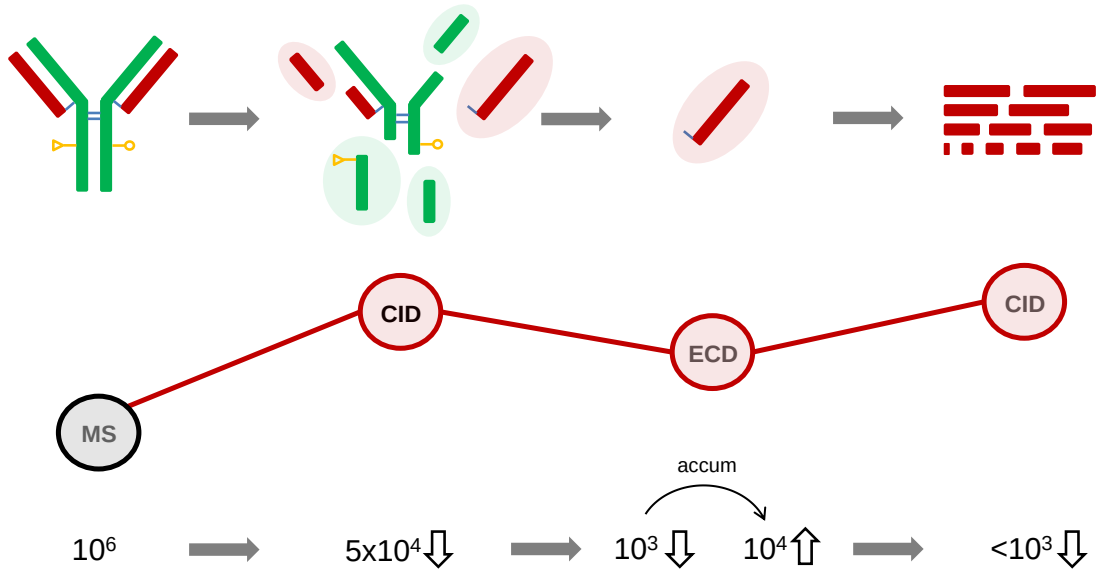

Figure 26. Ion accumulation mode is employed to enrich the population of fragment ions which are subjected to additional stages of ion activation dissociation.